6th IFAC Symposium on Mechatronic Systems
The International Federation of Automatic Control
April 10-12, 2013. Hangzhou, China

Self-tuning in Sliding Mode Control of High-Precision Motion Systems

Marcel F. Heertjes * **Yasemin Vardar** **

* *ASML, De Run, Veldhoven, The Netherlands (e-mail: marcel.heertjes@asml.com).*
** *Eindhoven University of Technology, Den Dolech 2, Eindhoven, The Netherlands (e-mail: y.vardar@student.tue.nl)*

Abstract: In high-precision motion systems, set-point tracking often comes with the problem of overshoot, hence poor settling behavior. To avoid overshoot, PD control (thus without using an integrator) is preferred over PID control. However, PD control gives rise to steady-state error in view of the constant disturbances acting on the system. To deal with both overshoot and steady-state error, a sliding mode controller with saturated integrator is studied. For large servo signals the controller is switched to PD mode as to constrain the integrator buffer and therefore the overshoot. For small servo signals the controller switches to PID mode as to avoid steady-state error. The tuning of the switching parameters will be done automatically with the aim to optimize the settling behavior. The sliding mode controller will be tested on a high-precision motion system.

Keywords: Motion systems, machine-in-the-loop optimization, self-tuning, sliding mode control, wafer scanners.

1. INTRODUCTION

Wafer scanners and their high-precision motion systems are used in the semiconductor industry for the production of integrated circuits (Butler, 2011). These systems need to be controlled to meet the demands on wafer position accuracy and throughput. Under proportional-integral-derivative (PID) control this generally poses the following problem. The integrator used to compensate for the unknown static disturbances gives rise to poor settling behavior (Seshagiri and Khalil, 2005a). This is because the integrator buffer created prior to scanning induces overshoot (or undershoot) at the beginning of the scanning interval. A solution to this problem would be to use PD control, but with the disadvantage that static disturbances induce steady-state errors in the scanning interval.

To deal with this trade-off the merits of sliding mode control will be studied (Hung et al., 1993; Menon and Khalil, 2010; Pisano and Usai, 2011; Seshagiri and Khalil, 2005b; Singh and Khalil, 2005; Young et al., 1999). More specifically, from Lee et al. (2011) and Nonaka and Sugizaki (2011) a saturated integrator design, or so-called integral sliding mode control, will be adopted. Instead of studying (for example) higher-order sliding mode control schemes like the twisting or super twisting algorithms studied by Salgado-Jiménez and Jouvencelet (2003); Janardhanan (2006), integral sliding mode control is studied because of its clear physical interpretation. For large servo signals, sufficiently removed from the sliding surface, the controller will operate in PD mode. This limits the integrator buffer, i.e. the overshoot/undershoot. Near the sliding surface, the controller operates in PID mode with the aim to avoid steady-state error.

Different from the designs in for example Boiko (2011); Eker (2006); Lee et al. (2011); Nonaka and Sugizaki (2011); Sam et al. (2004), the controller tunings in PD mode are done in frequency domain using manual loop shaping. Frequency-domain tunings directly link the control design to the physical understanding of the stage dynamics (resonances), closed-loop performance (bandwidths), and robust stability of the linear part of the closed-loop system (stability margins). The main contribution of this paper, however, are the tunings of the saturated integrator: the gain and the saturation length. This is done in time domain using a self-tuning algorithm, see also Hung et al. (2007); Kuo et al. (2007); Patete et al. (2008) for different approaches. The idea behind self-tuning is twofold. On the one hand, the nonlinear controller tunings do not follow from straightforward design and performance arguments (Nazrulla and Khalil, 2011). Self-tuning thus avoids trial-and-error in the tuning process. On the other hand, unknown disturbances and plant uncertainty generally require machine-specific tunings. Because the self-tuning algorithm combines model knowledge with time-series data, this requirement is automatically met.

The remainder of the paper is organized as follows. In Section II, a model of the motion system dynamics will be presented whereas in Section III, the sliding mode control design based on these dynamics will be discussed. In Section IV, tuning of the sliding mode controller will be considered. This involves self-tuning of the saturated feedback controller parameters in time-domain. In Section V, performance will be assessed through simulation and experiment. In Section VI, a summary of the main conclusions and observations will be given.

978-3-902823-31-1/13/$20.00 © 2013 IFAC

10.3182/20130410-3-CN-2034.00019

2. MODEL OF THE MOTION SYSTEM DYNAMICS

In wafer scanners, the scanning process is usually conducted with two simultaneously operating wafer positioning modules: one that is being exposed, and one that is being measured; see Shieh and Huang (2006); Xu and Li (2009) for piezoelectric motion systems in a similar control context. The servo control problem considered in this paper involves the exchange of these modules from measure to expose side and vice versa. Since the exchange interrupts the exposure process, minimizing settling times during this exchange directly aids to improved system performance in terms of wafer throughput.

2.1 Wafer Stage

A graphical representation of a wafer positioning module is shown in Fig.1. The module is part of an H-bridge struc-

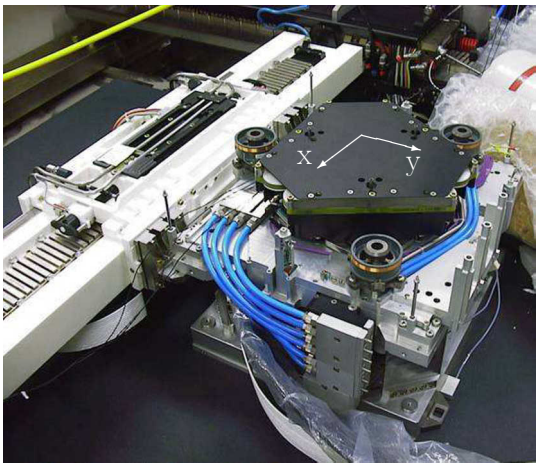

Fig. 1. A wafer positioning module.

ture which can move freely in x-direction along its center beam. In y-direction the center beam takes part in the motion, thereby inducing position-dependent behavior. Atop the course positioning module, a fine-positioning module is mounted which supports the wafer to be measured and exposed.

2.2 State-Space Model

For given time t and sampling time ΔT assume the dynamics of the positioning module in y-direction to be presented by the following (simplified and time-discretized) state-space model:

$$\begin{aligned} x_{\mathrm{p}}(t+\Delta T) &= A_{\mathrm{p}}x_{\mathrm{p}}(t) + B_{\mathrm{p}}u(t) \\ y(t) &= C_{\mathrm{p}}x_{\mathrm{p}}(t), \end{aligned} \tag{1}$$

with state vector $x_{\mathrm{p}}(t) \in \mathbb{R}^8$, $A_{\mathrm{p}} \in \mathbb{R}^{8\times 8}$, and $B_{\mathrm{p}}, C_{\mathrm{p}}^{\mathrm{T}} \in \mathbb{R}^8$, see (2) for the matrices; $u(t) \in \mathbb{R}$ represents a force applied to the system, whereas $y(t) \in \mathbb{R}$ represents the measured displacement resulting from this force.

2.3 Model Validation

The validity of the model in (1) and (2), which in frequency domain is given by:

$$Y(s) = \mathcal{P}(s)U(s), \tag{3}$$

with $Y(s), U(s) \in \mathbb{C}$ the Laplace transforms of $y(t), u(t) \in \mathbb{R}$, respectively, is shown in Fig.2. In Bode representation,

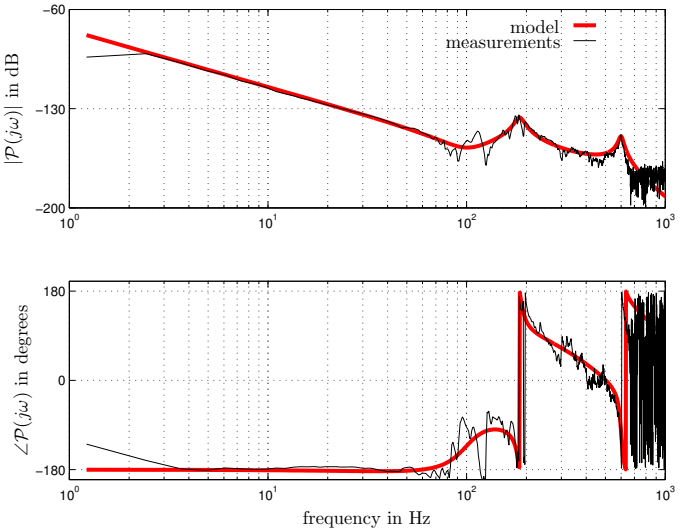

Fig. 2. Bode representation of the wafer positioning module $\mathcal{P}(j\omega)$.

a fair correspondence is obtained between the 8th order model and frequency response function measurements of $\mathcal{P}(j\omega) \in \mathbb{C}$. At low frequencies, double integrator behavior is shown, i.e. the positioning module can be characterized by a simple mass model. Beyond 60 Hz, however, the dynamics become more complex. For example, around 200 Hz the positioning module is largely decoupled from the actuators. Beyond 700 Hz, closed-loop identification induces poor measurement results. The same holds true below 3 Hz. As mentioned in Section 2.1, the system (by design) is position-dependent. Measuring $\mathcal{P}$ at different positions yields different characteristics. In minimizing settling times, it therefore makes sense to study integral sliding mode control as a means of nonlinear feedback which has the potential of adding position-dependent disturbance rejection properties to the closed-loop system.

3. INTEGRAL SLIDING MODE CONTROL DESIGN

For integral sliding mode control design we introduce the block diagram representation of Fig.3. By itself, the representation gives a clear physical interpretation of the controller structure. The wafer positioning module $\mathcal{P}$,

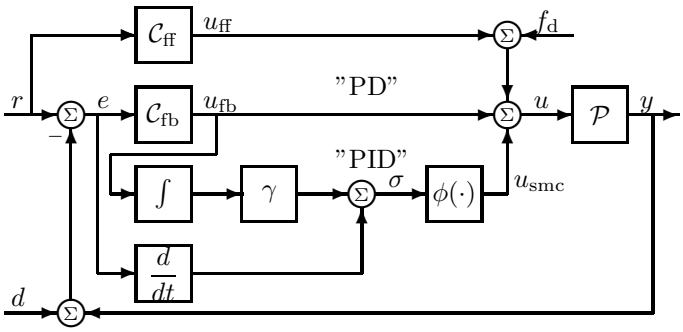

Fig. 3. Block diagram of the sliding mode control configuration.

which is (directly) subjected to input disturbances $f_d =$

$$A_{\mathrm{p}} = \begin{bmatrix} 6.164 & -1.056 & 4.204\ 10^{-1} & -1.059\ 10^{-1} & 3.431\ 10^{-2} & -1.383\ 10^{-2} & 6.253\ 10^{-3} & -1.202\ 10^{-3} \\ 16 & 0 & 0 & 0 & 0 & 0 & 0 & 0 \\ 0 & 4 & 0 & 0 & 0 & 0 & 0 & 0 \\ 0 & 0 & 4 & 0 & 0 & 0 & 0 & 0 \\ 0 & 0 & 0 & 2 & 0 & 0 & 0 & 0 \\ 0 & 0 & 0 & 0 & 1 & 0 & 0 & 0 \\ 0 & 0 & 0 & 0 & 0 & 0.5 & 0 & 0 \\ 0 & 0 & 0 & 0 & 0 & 0 & 0.5 & 0 \end{bmatrix} \tag{2}$$

$$B_{\mathrm{p}} = \begin{bmatrix} 3.815\ 10^{-6} & 0 & 0 & 0 & 0 & 0 & 0 & 0 \end{bmatrix}^{\mathrm{T}}$$

$$C_{\mathrm{p}} = \begin{bmatrix} 2.897\ 10^{-6} & -7.012\ 10^{-7} & -4.721\ 10^{-8} & 1.55\ 10^{-7} & -3.628\ 10^{-9} & -8.732\ 10^{-8} & 9.241\ 10^{-9} & 1.30\ 10^{-7} \end{bmatrix}$$

$f_d(t) \in \mathbb{R}$ and (indirectly) to output disturbances $d = d(t) \in \mathbb{R}$, is controlled by a sliding mode controller which consists of three parts: a feedforward part $u_{\mathrm{ff}} = u_{\mathrm{ff}}(t) \in \mathbb{R}$ with feedforward controller $\mathcal{C}_{\mathrm{ff}}$, a linear feedback part $u_{\mathrm{fb}} = u_{\mathrm{fb}}(t) \in \mathbb{R}$ with feedback controller $\mathcal{C}_{\mathrm{fb}}$, and a saturated feedback part $u_{\mathrm{smc}} = u_{\mathrm{smc}}(t) \in \mathbb{R}$; see Amer et al. (2011); Tsuruta et al. (2011); Xi et al. (2010) for other designs but with a comparable structure.

For saturated feedback let us first adopt the control design from Nonaka and Sugizaki (2011) and then adapt this design toward the specific needs of the considered stage application. In Nonaka and Sugizaki (2011) the input signal $\sigma = \sigma(t) \in \mathbb{R}$ is mapped onto a saturation function: $\sigma(t) \mapsto \phi(\sigma(t))$, giving

$$u_{\mathrm{smc}}(t) = \phi(\sigma(t)) = \kappa \mathrm{sat}(\sigma(t)), \tag{4}$$

$\kappa \geq 0$ a gain, and

$$\mathrm{sat}(\sigma(t)) \stackrel{\mathrm{def}}{=} \begin{cases} \dfrac{\sigma(t)}{\epsilon}, & \text{if} |\sigma(t)| \leq \epsilon, \\ \mathrm{sign}(\sigma(t)), & \text{otherwise}, \end{cases} \tag{5}$$

with $\epsilon > 0$. The input signal $\sigma = \sigma(t) \in \mathbb{R}$ reads:

$$\sigma(t) = \frac{de(t)}{dt} + \gamma \int_0^t u_{\mathrm{fb}}(\tau) d\tau, \tag{6}$$

with $\gamma > 0$ a gain and the error signal $e = e(t) \in \mathbb{R}$:

$$e(t) = r(t) - y(t) - d(t). \tag{7}$$

Now assume that $\mathcal{P}$ is a double integrator plant, which is partly validated in Fig.2, or

$$y(t) = \frac{1}{m} \iint_R u(\tau) d\tau, \tag{8}$$

with region $R = [0, t] \times [0, t]$ and mass $m > 0$. Moreover, let $\mathcal{C}_{\mathrm{fb}}$ satisfy:

$$u_{\mathrm{fb}}(t) = k_{\mathrm{p}} e(t) + k_{\mathrm{v}} \frac{de(t)}{dt}, \tag{9}$$

with gain k_{p} for the proportional term and gain k_{v} for the velocity term, respectively, whereas $\mathcal{C}_{\mathrm{ff}}$ satisfies:

$$u_{\mathrm{ff}}(t) = m \frac{d^2 r(t)}{dt^2}. \tag{10}$$

Fig.3 thus shows that $\mathcal{C}_{\mathrm{ff}}$ should match with the inverse plant characteristics $\mathcal{P}^{-1}$, $\mathcal{C}_{\mathrm{fb}}$ gives a "PD" controller contribution, and depending on $\phi(\cdot)$ an extra "PID" controller contribution will be applied to the system.

Stability of the control design follows from Lyapunov arguments. Namely for initial conditions: $e(0) = de(0)/dt = 0$, it follows from Fig.3 and using (9) that:

$$\sigma(t) = \gamma k_{\mathrm{p}} \int_{\tau=0}^{t} e(\tau) d\tau + \gamma k_{\mathrm{v}} e(t) + \frac{de(t)}{dt}. \tag{11}$$

Substitution of (8) in (7) and considering the second derivatives it then follows for $\gamma = 1/m$ and

$$u(t) = u_{\mathrm{ff}}(t) + u_{\mathrm{fb}}(t) + u_{\mathrm{smc}}(t) + f_{\mathrm{d}}(t), \tag{12}$$

see Fig.3, that $d\sigma(t)/dt$ can be written as

$$\frac{d\sigma(t)}{dt} = -\frac{\kappa}{m} \mathrm{sat}(\sigma(t)) - \frac{d^2 d(t)}{dt^2} - \frac{1}{m} f_{\mathrm{d}}(t). \tag{13}$$

By defining the Lyapunov function candidate:

$$V(t) = \sigma^2(t), \tag{14}$$

which for $\sigma(t) \neq 0$ is positive definite, it follows that:

$$\begin{aligned} \frac{dV(t)}{dt} &= 2 \frac{d\sigma(t)}{dt} \sigma(t) \\ &= -\frac{2\kappa}{m} \mathrm{sat}(\sigma(t)) \sigma(t) - 2 \frac{d^2 d(t)}{dt^2} \sigma(t) - \frac{2}{m} f_{\mathrm{d}}(t) \sigma(t). \end{aligned} \tag{15}$$

If the disturbances acting on the system are uniformly bounded, or

$$\left| \frac{d^2 d(t)}{dt} + \frac{1}{m} f_{\mathrm{d}}(t) \right| < \frac{\kappa}{m}, \ t \in [0, \infty), \tag{16}$$

which requires the gain κ to be chosen large enough to suppress these disturbances, it follows for $|\sigma(t)| > \epsilon$ and substitution of (5) that:

$$\frac{dV(t)}{dt} \leq -\frac{\kappa}{m} |\sigma(t)| + \left| \frac{d^2 d(t)}{dt} + \frac{1}{m} f_{\mathrm{d}}(t) \right| |\sigma(t)| < 0, \tag{17}$$

which leaves $|\sigma(t)| \leq \epsilon$ a positively invariant set to which all solutions $\sigma(t) \in \mathbb{R}$ converge.

For stage control, the sliding mode control design described above needs modification. On the one hand, the feedforward controller $\mathcal{C}_{\mathrm{ff}}$ in (10) is generally a too simplified representation of the inverse plant dynamics $\mathcal{P}$ in Fig.2. Namely $\mathcal{P}$ is dominated by higher-order dynamics that should be addressed as to improve the effectiveness of the inertia-based feedforward controller in (10). On the other hand, closed-loop stability in the case of $\phi(\sigma) = 0$, $\forall \sigma \in \mathbb{R}$, i.e. with "PD" control only, is not necessarily satisfied for $\mathcal{P}$ in Fig.2 (Boiko, 2011; Daly and Wang, 2009; Zeinali and Notash, 2010). For example, Fig.2 shows much more phase lag then is being described by (8).

The feedforward controller $\mathcal{C}_{\mathrm{ff}}$ resulting from (10) is modified as follows. Because the reference signal $r(t)$ is known in advance, its second time derivative $a(t)$ is known in advance too, such that:

$$u_{\rm ff}(t) = ma(t). \tag{18}$$

Using (18) avoids unnecessary time-delay in the discrete-time computation of the feedforward compensation $u_{\rm ff}(t) \in \mathbb{R}$. Unfortunately, $u_{\rm ff}(t)$ needs to be time-delayed anyway in order to synchronize with the forces $u_{\rm fb}(t), u_{\rm smc}(t) \in \mathbb{R}$, or:

$$U_{\rm ff}(s) = \mathcal{C}_{\rm ff}(s)A(s),\ \mathcal{C}_{\rm ff}(s) = m\exp^{-\delta\Delta Ts}, \tag{19}$$

with $U_{\rm ff}(s)$, $A(s) \in \mathbb{C}$ the Laplace transforms of $u_{\rm ff}(t)$, $a(t) \in \mathbb{R}$, respectively, $\delta = 3$, and $\Delta T = 1/5000$ s. In view of the position-dependent dynamics of the stage system, modifications toward higher-order feedforward control are not considered in this paper. In fact, the presence of position-dependent dynamics forms the main motivation to use integral sliding mode control as a means to improve upon the settling behavior of the stage system.

The feedback controller $\mathcal{C}_{\rm fb}(s) \in \mathbb{C}$ in:

$$U_{\rm fb}(s) = \mathcal{C}_{\rm fb}(s)E(s), \tag{20}$$

with $U_{\rm fb}(s)$, $E(s) \in \mathbb{C}$ the Laplace transforms of $u_{\rm fb}(t)$, $e(t) \in \mathbb{R}$, respectively, is modified by manual loop-shaping. In addition to (9) with $k_{\rm p} = 10^6$ Nm^{-1} and $k_{\rm v} = k_{\rm p}/(24\pi)$ Nsm^{-1}, three loop-shaping filters are added: a second-order low-pass filter with a cut-off frequency at 120 Hz and two second-order notch filters tuned around the plant resonances at 115 and 200 Hz, see also Fig.2. Note that output feedback is used instead of state feedback. For the considered stage application, output feedback is the most logical choice because of the limited set of actuators and sensors used for control. Moreover, the PD-like controller $\mathcal{C}_{\rm fb}(s) \in \mathbb{C}$ with extra second-order filters reflects a clear physical understanding in tuning given the suppression of plant resonances (notch filters) and high-frequency noise attenuation (low-pass filter).

In time-domain, the controller is given by the state-space model:

$$\begin{aligned} x_{\rm c}(t+\Delta T) &= A_{\rm c}x_{\rm c}(t) + B_{\rm c}e(t) \\ u_{\rm fb}(t) &= C_{\rm c}x_{\rm c}(t), \end{aligned} \tag{21}$$

with state vector $x_{\rm c}(t) \in \mathbb{R}^8$, $A_{\rm c} \in \mathbb{R}^{8\times 8}$, and $B_{\rm c}, C_{\rm c}^{\rm T} \in \mathbb{R}^8$; see (22) for the matrices.

The need for loop shaping is shown in the Nyquist plots of Fig.4. By depicting the measured open-loop characteristics, $\mathcal{C}_{\rm fb}(j\omega)\mathcal{P}(j\omega) \in \mathbb{C}$, either with (9) in black or with (21) in red, it can be seen that robust stability and performance of the linear part of the sliding mode control design is obtained for (21); see Kuo et al. (2008) for an adaptive approach toward the controller tunings. Fig.4 also shows that (9) renders the sliding mode control design much less robust, hence the need for loop shaping.

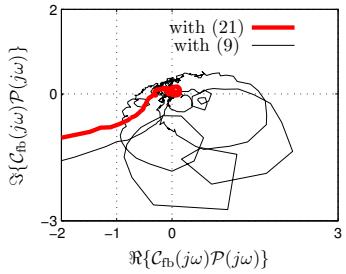

Fig. 4. Nyquist plot of the openloop $\mathcal{C}_{\rm fb}(j\omega)\mathcal{P}(j\omega)$.

Having tuned the feedforward part and the linear feedback part in Fig.3 using frequency domain techniques, the (nonlinear) saturated feedback part will be tuned in time domain. This is because tunings of the parameters of the saturation function do not seriously affect the stability properties of the closed-loop system: for large enough input $\sigma(t) \in \mathbb{R}$, the system falls back onto the "stable" PD mode. These tunings, however, do influence closed-loop performances, which differ from machine to machine and therefore can best be tuned in time-domain using data from said machines.

4. INTEGRAL SLIDING MODE CONTROL TUNING

With integral sliding mode control tuning we mean self-tuning of the parameters $\kappa, \epsilon \in \mathbb{R}$ of the saturation function $\phi(\cdot)$ in (4). Tuning of the controller parameters is essential in terms of achieving tracking performance (Nazrulla and Khalil, 2011; Tannuri et al., 2010). For this purpose, the data-driven approach from Heertjes and Nijmeijer (2012) is followed that explicitly addresses the saturation nonlinearity. In this approach, the lifted system description from Bamieh et al. (1991) provides the means to compute the gradient error signals from the sampled data obtained from a particular experiment. These gradient error signals are used to compute an update of the controller parameters (by Newton optimization) for the next experiment. In so doing, machine specific tunings will be obtained inducing dedicated machine performances.

More specifically, the aim in self-tuning is to iteratively find the set of switching control parameters $p_{\rm opt} = [\kappa_{\rm opt}, \epsilon_{\rm opt}]^{\rm T}$ that minimizes the performance-relevant servo error signals $e(t) \in \mathbb{R}$ in the time interval $t \in [t_1, t_2]$, or

$$p_{\rm opt} \stackrel{\rm def}{=} \arg\min_{p} \int_{t_1}^{t_2} e^2(t)dt, \tag{23}$$

with $p = p_k = [\kappa_k, \epsilon_k]^{\rm T}$ and $k \in \mathbb{N}^+$ the iteration number. To find $p_{\rm opt}$, consider the Gauss-Newton scheme [1]:

$$p_{k+1} = p_k + \beta\left({\mathbf{p}_k}^{\rm T}\mathbf{p}_k\right)^{-1}{\mathbf{p}_k}^{\rm T}\mathbf{e}_k, \tag{24}$$

where $0 < \beta \leq 1$ is a damping coefficient, $\mathbf{p}_k \in \mathbb{R}^{n\times 2}$ contains the n-sampled gradient error signals:

$$\mathbf{p}_k = \left[\frac{\partial \mathbf{e}_k}{\partial \kappa_k}\ \frac{\partial \mathbf{e}_k}{\partial \epsilon_k}\right], \tag{25}$$

and $\mathbf{e}_k \in \mathbb{R}^n$ represents the data-sampled error signal:

$$\mathbf{e}_k = [e_k(t_1)\ e_k(t_1+\Delta T)\ \ldots\ e_k(t_2)]^{\rm T}, \tag{26}$$

with $t_2 = t_1 + (n-1)\Delta T$ and the subscript k denoting the k-th realization of the considered signal or parameter. In (24), $\mathbf{e}_k \in \mathbb{R}^n$ can directly be obtained from time-series measurement or simulation. This does not hold true for the gradient error signals in (25). To obtain these gradients, the system of Fig.3 is split up in two parts: a part from output $u_{\rm smc}(t)$ to input $\sigma(t)$ which consists of linear dynamics only, and a part containing the nonlinearity, i.e. the saturation function $\phi(\cdot)$ in (4).

The linear part of the system follows from (19), (20), and:

[1] In the case that the Gauss-Newton scheme induces numerical conditioning problems in computing the (approximative) Hessian, the Levenberg-Marquardt scheme may prove beneficial. As a drawback, the latter often associates with reduced convergence rates.

$$A_{\rm c} = \begin{bmatrix} 7.336 & -7.385\ 10^{-1} & 1.705\ 10^{-1} & -9.882\ 10^{-2} & 3.679\ 10^{-2} & -1.718\ 10^{-2} & 9.207\ 10^{-3} & -8.667\ 10^{-3} \\ 32 & 0 & 0 & 0 & 0 & 0 & 0 & 0 \\ 0 & 8 & 0 & 0 & 0 & 0 & 0 & 0 \\ 0 & 0 & 2 & 0 & 0 & 0 & 0 & 0 \\ 0 & 0 & 0 & 2 & 0 & 0 & 0 & 0 \\ 0 & 0 & 0 & 0 & 1 & 0 & 0 & 0 \\ 0 & 0 & 0 & 0 & 0 & 0.5 & 0 & 0 \\ 0 & 0 & 0 & 0 & 0 & 0 & 0.125 & 0 \end{bmatrix} \tag{22}$$

$$B_{\rm c} = \begin{bmatrix} 256 & 0 & 0 & 0 & 0 & 0 & 0 & 0 \end{bmatrix}^{\rm T}$$

$$C_{\rm c} = \begin{bmatrix} 2.511\ 10^{2} & -4.477\ 10^{1} & 1.361\ 10^{1} & -9.133 & 3.656 & -1.752 & 9.389\ 10^{-1} & -8.838\ 10^{-1} \end{bmatrix}$$

$$\Sigma(s) = \frac{\gamma U_{\rm fb}(s)}{s} + sE(s) \tag{27a}$$
$$E(s) = R(s) - D(s) - Y(s) \tag{27b}$$
$$Y(s) = \mathcal{P}(s)U(s) \tag{27c}$$
$$U(s) = F_{\rm d}(s) + U_{\rm ff}(s) + U_{\rm fb}(s) + U_{\rm smc}(s), \tag{27d}$$

with $\Sigma(s) \in \mathbb{C}$ the Laplace transform of $\sigma(t) \in \mathbb{R}$. By substitution, it can be derived that:

$$\begin{aligned} \Sigma(s) = {} & \mathcal{S}_{\rm mod}(s)(R(s) - D(s)) \\ & - \mathcal{S}^{\rm p}_{\rm mod}(s)(U_{\rm ff}(s) + F_{\rm d}(s) + U_{\rm smc}(s)), \end{aligned} \tag{28}$$

with the modified (closed-loop) sensitivity and process sensitivity function, respectively, defined as:

$$\begin{aligned} \mathcal{S}_{\rm mod}(s) &= \frac{\gamma \mathcal{C}_{\rm fb}(s) + s^2}{s + s\mathcal{P}(s)\mathcal{C}_{\rm fb}(s)} \\ \mathcal{S}^{\rm p}_{\rm mod}(s) &= \mathcal{P}(s)\mathcal{S}_{\rm mod}(s). \end{aligned} \tag{29}$$

It is assumed that $\mathcal{S}_{\rm mod}(s), \mathcal{S}^{\rm p}_{\rm mod}(s) \in \mathbb{C}$ are strictly proper transfer functions, which is reasonable for the considered double integrator-based motion systems. Since $\mathcal{C}_{\rm fb} \in \mathbb{C}$ is chosen to stabilize $\mathcal{P}(s) \in \mathbb{C}$, $\mathcal{S}_{\rm mod}, \mathcal{S}^{\rm p}_{\rm mod}$ are stable by design. In state-space representation, Eq.(28) reads:

$$\begin{aligned} x_{\rm d}(t + \Delta T) &= A_{\rm d}x_{\rm d}(t) + B_{\rm d,1}v(t) - B_{\rm d,2}(w(t) + u_{\rm smc}(t)) \\ \sigma(t) &= C_{\rm d}x_{\rm d}(t), \end{aligned} \tag{30}$$

with state vector $x_{\rm d} = x_{\rm d}(t) \in \mathbb{R}^m$, $A_{\rm d} \in \mathbb{R}^{m \times m}$ Hurwitz, $B_{\rm d,1}, B_{\rm d,2}, C_{\rm d}^{\rm T} \in \mathbb{R}^m$, the pairs $(A_{\rm d}, B_{\rm d,1})$ and $(A_{\rm d}, B_{\rm d,2})$ being state controllable, the pair $(A_{\rm d}, C_{\rm d})$ being state observable, and $v(t) = r(t) - d(t)$, $w(t) = u_{\rm ff}(t) + f_{\rm d}(t)$.

For $x_{\rm d}(t_1) = 0$, Eq.(30) can be put in lifted form:

$$\begin{bmatrix} \sigma_k(t_1) \\ \vdots \\ \sigma_k(t_2) \end{bmatrix} = \overbrace{\begin{bmatrix} 0 & & \cdots & 0 \\ C_{\rm d}B_{\rm d,1} & & & \vdots \\ \vdots & \ddots & \ddots & \\ C_{\rm d}A_{\rm d}^{n-2}B_{\rm d,1} & \cdots & C_{\rm d}B_{\rm d,1} & 0 \end{bmatrix}}^{\mathbf{S}_{\rm mod}} \begin{bmatrix} v_k(t_1) \\ \vdots \\ v_k(t_2) \end{bmatrix}$$
$$- \overbrace{\begin{bmatrix} 0 & 0 & \cdots & 0 \\ C_{\rm d}B_{\rm d,2} & & & \vdots \\ \vdots & \ddots & \ddots & 0 \\ C_{\rm d}A_{\rm d}^{n-2}B_{\rm d,2} & \cdots & C_{\rm d}B_{\rm d,2} & 0 \end{bmatrix}}^{\mathbf{S}^{\rm p}_{\rm mod}} \begin{bmatrix} w_k(t_1) + u_{\rm smc,k}(t_1) \\ \vdots \\ w_k(t_2) + u_{\rm smc,k}(t_2) \end{bmatrix}, \tag{31}$$

which gives rise to the following algebraic expression:

$$\boldsymbol{\sigma}_k = -\mathbf{S}^{\rm p}_{\rm mod}\mathbf{u}_{{\rm smc},k} + \mathbf{S}_{\rm mod}\mathbf{v}_k - \mathbf{S}^{\rm p}_{\rm mod}\mathbf{w}_k, \tag{32}$$

with the data-sampled signals $\boldsymbol{\sigma}_k = [\sigma_k(t_1) \dots \sigma_k(t_2)]^{\rm T}$, $\mathbf{v}_k = [v_k(t_1) \dots v_k(t_2)]^{\rm T}$, $\mathbf{w}_k = [w_k(t_1) \dots w_k(t_2)]^{\rm T} \in \mathbb{R}^n$, σ_k, v_k, and w_k being k-th realizations of the signals σ, v, and w, respectively, and Toeplitz matrices: $\mathbf{S}_{\rm mod}, \mathbf{S}^{\rm p}_{\rm mod} \in \mathbb{R}^{n \times n}$, representing the modified sensitivity and process sensitivity dynamics.

For the nonlinear part of the system write:

$$\mathbf{u}_{{\rm smc},k} = \boldsymbol{\phi}(\boldsymbol{\sigma}_k), \tag{33}$$

with the saturation-based nonlinearity decomposed into:

$$\boldsymbol{\phi}(\boldsymbol{\sigma}_k) = \frac{\kappa_k}{\epsilon_k}\boldsymbol{\phi}_1(\boldsymbol{\sigma}_k)\boldsymbol{\sigma}_k + \kappa_k\boldsymbol{\phi}_2(\boldsymbol{\sigma}_k), \tag{34}$$

$\boldsymbol{\phi}_1(\boldsymbol{\sigma}_k) \in \mathbb{R}^{n \times n}$ a positive semi-definite diagonal matrix:

$$\boldsymbol{\phi}_1(\boldsymbol{\sigma}_k)[i,i] = \begin{cases} 1, & \text{if} |\sigma_k(t_1 + (i-1)\Delta T)| \leq \epsilon_k, \\ 0, & \text{otherwise}, \end{cases} \tag{35}$$

for $i \in \{1 \dots n\}$ and $\boldsymbol{\phi}_2(\boldsymbol{\sigma}_k) \in \mathbb{R}^n$ given by:

$$\boldsymbol{\phi}_2(\boldsymbol{\sigma}_k)[i] = \begin{cases} 0, & \text{if} |\sigma_k(t_1 + (i-1)\Delta T)| \leq \epsilon_k, \\ \text{sign}(\sigma_k(t_1 + (i-1)\Delta T)), & \text{otherwise}. \end{cases} \tag{36}$$

Combining (32), (33), (34) and using the linear relation from $e(t)$ to $\sigma(t)$ (see Fig.3) which in Laplace domain follows from substitution of (20) in (27a), it follows (after some algebra [2]) that:

$$\begin{aligned} \frac{\partial \mathbf{e}_k}{\partial \kappa_k} &= -A(\boldsymbol{\phi}_1(\boldsymbol{\sigma}_k)\boldsymbol{\sigma}_k + \epsilon_k\boldsymbol{\phi}_2(\boldsymbol{\sigma}_k)) \\ \frac{\partial \boldsymbol{\sigma}_k}{\partial \epsilon_k} &= \frac{\kappa_k}{\epsilon_k}A\boldsymbol{\phi}_1(\boldsymbol{\sigma}_k)\boldsymbol{\sigma}_k, \end{aligned} \tag{37}$$

with

$$A = (I + \kappa\mathbf{S}^{\rm p}_{\rm mod}\boldsymbol{\phi}_1(\boldsymbol{\sigma}_k))^{-1}\mathbf{S}^{\rm p}, \tag{38}$$

and $\mathbf{S}^{\rm p} \in \mathbb{R}^{n \times n}$ a Toeplitz matrix similar to $\mathbf{S}^{\rm p}_{\rm mod} \in \mathbb{R}^{n \times n}$ but based on the unmodified process sensitivity function:

$$\mathcal{S}^{\rm p}(s) = \frac{\mathcal{P}(s)}{1 + \mathcal{P}(s)\mathcal{C}_{\rm fb}(s)}. \tag{39}$$

5. PERFORMANCE ASSESSMENT

Performance of the (modified) sliding mode control design from Section 3 is assessed in two parts. Firstly, settings for the saturation parameters κ and ϵ are found from simulations using the self-tuning procedure described in Section 4, and, secondly, control performance is demonstrated for these settings via measurement results.

[2] The main property used in the derivation of (37) is given by the fact that $\sigma_k(i)\partial\boldsymbol{\phi}_1(\boldsymbol{\sigma}_k)[i,i]/\partial\epsilon_k + \epsilon_k\partial\boldsymbol{\phi}_2(\boldsymbol{\sigma}_k)[i]/\partial\epsilon_k = 0$.

Using the models and algorithms from the previous sections, the results from parameter optimization are summarized in Fig.5. It can be seen that the squared error

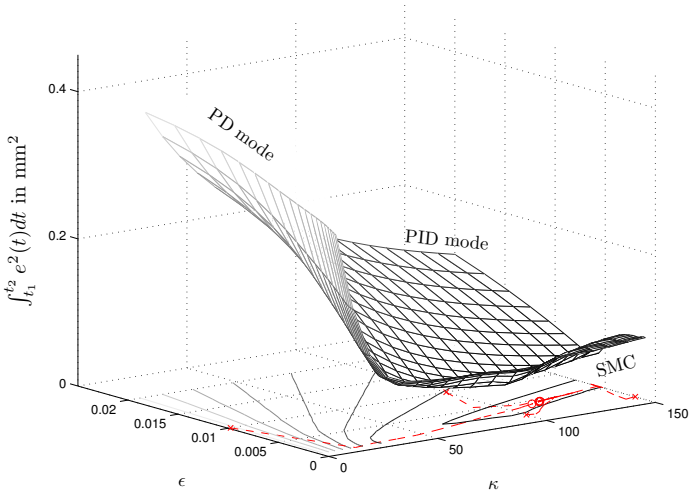

Fig. 5. Cost function evaluation in (23) from time-series simulations with $\kappa \in \{0, 150\}$ and $\epsilon \in \{0.001, 0.02\}$.

evaluation from (23) in the performance interval $t \in [t_1, t_2]$ with $t_1 = 0$ s and $t_2 = 0.15$ s (see also Fig.6) yields a small region of minima with different combinations of κ and ϵ. It is clear that κ needs to be large enough to cope with the (static) disturbances as stated in (16). Moreover beyond a threshold value of $\kappa \approx 25$ both κ and $1/\epsilon$ effectively represent controller gain and thus are interchangeable: larger values for κ correspond to smaller values for $1/\epsilon$ in maintaining roughly the same control performance. It is also clear that best performance is obtained with the saturated integrator rather than operating in either "PD" or "PID" mode. For $\epsilon \to 0$, so if (5) tends to a signum function, sliding mode control induces deteriorated performance (chattering) in the considered metric; see Laghrouche et al. (2007) regarding a solution based on higher-order sliding mode control. Fig.5 also shows that for four sets of initial conditions (denoted by the $\times$-symbols) optimized sets $p_{\text{opt}} \in \mathbb{R}^2$ are found around $\kappa \approx 115$ and $\epsilon \approx 0.0045$ (denoted by the $\circ$-symbols); in the optimization $k = 15$ and $\beta = 0.4$.

With $\kappa = 100$ and $\epsilon = 0.005$, the results of time-series simulation (upper part) and measurement on an industrial wafer scanner (lower part) are shown in Fig.6. Given a (scaled) acceleration set-point (dashed curve), the error responses are depicted for PID mode, PD mode, and integral sliding mode control (SMC). Compared with PID control, PD control induces less overshoot but yields steady-state error. Integral sliding mode control (SMC) induces less overshoot (and undershoot) but without having steady-state error. This gives improved settling behavior in terms of the considered wafer exchange problem.

6. CONCLUSIONS

To improve settling performance of high-precision motion systems, a (modified) integral sliding mode control design is considered. The design switches between PD mode, which aims at less overshoot, and PID mode, which induces no steady-state error. The switching parameters are

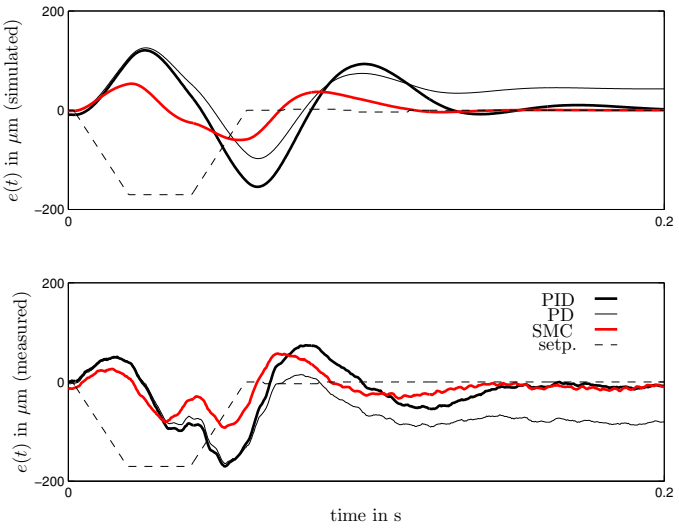

Fig. 6. Time-series simulations and measurements in PID mode, PD mode, and SMC ($\kappa = 100$ and $\epsilon = 0.005$).

found by self-tuning. Herein a machine-in-the-loop optimization scheme is used which incorporates, on the one hand, model knowledge of the plant and the controller and, on the other hand, servo error data containing the effect of disturbances and plant uncertainty. The effectiveness of the modified design and its tunings is demonstrated by simulations and experimental results. Self-tuning in experiment as well as the stability properties of the modified design and optimization scheme will be addressed in future work.

REFERENCES

A.F. Amer, E.A. Sallam, and W.M. Elawady. Adaptive fuzzy sliding mode control using supervisory fuzzy control for 3 DOF planar robot manipulators. Applied Soft Computing, 11:4943-4953, 2011.

B. Bamieh, P.J. Boyd, B.A. Francis, and A. Tannenbaum. A lifting technique for linear periodic systems with applications to sampled-data control. Systems and Control Letters, 17:79-88, 1991.

M. Boiko. Analysis of chattering in sliding mode control systems with continuous boundary layer approximation of discontinuous control. In Proceedings of the American Control Conference, San Francisco, CA, USA:757-762, 2011

H. Butler. Position control in lithographic equipment; an enabler for current-day chip manufacturing. IEEE Control Systems Magazine, 11:28-47, 2011.

B. Castillo-Toledo, S. Di Gennaro, A.G. Loukianov, and J. Rivera. Discrete time sliding mode control with application to induction motors. Automatica, 44:3036-3045, 2008.

J.M. Daly JM and D.W.L. Wang. Output feedback sliding mode control in the presence of unknown disturbances. System & Control Letters, 58:188-193, 2009.

I. Eker. Sliding mode control with PID sliding surface and experimental application to an electromechanical plant. ISA Transactions, 45(1):109-118, 2006.

M.F. Heertjes and H. Nijmeijer. Self-tuning of a switching controller for scanning motion systems. Mechatronics, 22:310-319, 2012.

L.-C. Hung, H.-P. Lin, and H.-Y. Chung. Design of self-tuning fuzzy sliding mode control for TORA system. Expert Systems with Applications, 32:201-212, 2007.

J.Y. Hung, W. Gao, and J.C. Hung. Variable structure control: a survey. Transactions on Industrial Electronics, 40(1):2-22, 1993.

S. Janardhanan. Relay-free second order sliding mode control. IEEE International Conference on Industrial Technology, Mumbai, India: 2206-2210,2006.

T.C. Kuo, Y.J. Huang, and S.H. Chang. Sliding mode control with self-tuning law for uncertain nonlinear systems. ISA Transactions, 47:171-178, 2007.

T.C. Kuo, Y.J. Huang, C.Y. Chen, and S.H. Chang. Adaptive sliding mode control with PID tuning for uncertain systems. Engineering Letters, 16(3):1-5, 2008.

S. Laghrouche, F. Plestan, and A. Glumineau. Higher order sliding mode control based on integral sliding mode. Automatica, 43:531-537, 2007.

W.R. Lee, J.H. Lee, and K.H. You. Augmented sliding-mode control of an ultra-precision positioning system. Precision Engineering, 35:521-524, 2011.

A.Y. Memon and H.K. Khalil. Output regulation of nonlinear systems using conditional servocompensators. Automatica, 46:1119-1128, 2010.

S. Nazrulla and H.K. Khalil. Robust stabilization of non-minimum phase nonlinear systems using extended high-gain observers. Transactions on Automatic Control, 56(4):802-813, 2011.

K. Nonaka and H. Sugizaki. Integral sliding mode altitude control for a small model helicopter with ground effect compensation. In Proceedings of the American Control Conference, San Francisco, CA, USA:202-207, 2011.

A. Patete, K. Furuta, and M. Tomizuka. Self-tuning control based on generalized minimum variance criterion for auto-regressive models. Automatica, 44:1970-1975, 2008.

A. Pisano and E. Usai. Sliding mode control: a survey with applications in math. Mathematics and Computers in Simulation, 81:954-979, 2011.

T. Salgado-Jiménez and B. Jouvencelet. Using a high order sliding modes for diving control a torpedo autonomous underwater vehicle. In Proceedings of the Oceans 2003 MTS/IEEE Conference, San Diego, CA: 934-939, 2003.

Y.Md. Sam, J.H.S. Osman, and M.R.A. Ghani. A class of proportional-integral sliding mode control with application to active suspension system. System & Control Letters, 51:217-223, 2004.

S. Seshagiri S and H.K. Khalil. Robust output feedback regulation of minimum-phase nonlinear systems using conditional integrators. Automatica, 41:43-54, 2005.

S. Seshagiri S and H.K. Khalil. Robust output regulation of minimum phase nonlinear systems using conditional servocompensators. International Journal of Robust and Nonlinear Control, 15:83-102, 2005.

H.-J. Shieh and P.-K. Huang. Trajectory tracking of piezoelectric positioning stages using a dynamic sliding-mode control. Transactions on Ultrasonics, Ferroelectrics, and Frequency Control, 53(10):1872-1882, 2006.

A. Singh and H.K. Khalil. Regulation of nonlinear systems using conditional integrators. International Journal of Robust and Nonlinear Control, 15:339-362, 2005.

E.A. Tannuri, A.C. Agostinho, H.M. Morishita, and L. Moratelli Jr. Dynamic positioning systems: an experimental analysis of sliding mode control. Control Engineering Practice, 18:1121-1132, 2010.

K. Tsuruta, K. Sato, and T. Fujimoto. High-speed and high-precision position control using a nonlinear compensator. Book Chapter in Advances in PID Control Control. Editor: Valery D. Yurkevich, In Tech: 143-166, 2011.

X.-C. Xi, G.-S. Hong, and A.-N. Poo. Improving cnc contouring accuracy by integral sliding mode control. Mechatronics, 20:445-452, 2010.

Q. Xu and Y. Li. Dynamics modeling and sliding mode control of an xy micropositioning stage. In Proceedings of the International Symposium on Robot Control, Gifu, Japan:781-786, 2009.

X.-G. Yan, S.K. Spurgeon, and C. Edwards. Sliding mode control for time-varying delayed systems based on a reduced-order observer. Automatica, 46:1354-1362, 2010.

K.D. Young, V.I. Utkin, and Ü. Özgüner. A control engineer's guide to sliding mode control. Transactions on control systems technology, 7(3):328-342, 1999.

M. Zeinali and L. Notash. Adaptive sliding mode control with uncertainty estimator for robot manipulators. Mechanism and Machine Theory, 45:80-90, 2010.